JACS
JOURNAL OF THE AMERICAN CHEMICAL SOCIETY
Article
pubs.acs.org/JACS

The Mechanism of N−N Double Bond Cleavage by an Iron(II) Hydride Complex

Sarina M. Bellows,[†] Nicholas A. Arnet,[‡] Prabhuodeyara M. Gurubasavaraj,[†,⊥] William W. Brennessel,[†] Eckhard Bill,[§] Thomas R. Cundari,[∥] and Patrick L. Holland*[,†,‡]

[†]Department of Chemistry, University of Rochester, Rochester, New York 14627, United States
[‡]Department of Chemistry, Yale University, New Haven, Connecticut 06520, United States
[§]Max Planck Institute for Chemical Energy Conversion, Stiftstrasse 34-36, 45470 Mülheim an der Ruhr, Germany
[∥]Department of Chemistry and CASCaM, University of North Texas, Denton, Texas 76203, United States

Supporting Information

ABSTRACT: The use of hydride species for substrate reductions avoids strong reductants, and may enable nitrogenase to reduce multiple bonds without unreasonably low redox potentials. In this work, we explore the N═N bond cleaving ability of a high-spin iron(II) hydride dimer with concomitant release of H_2. Specifically, this diiron(II) complex reacts with azobenzene (PhN═NPh) to perform a four-electron reduction, where two electrons come from H_2 reductive elimination and the other two come from iron oxidation. The rate law of the H_2 releasing reaction indicates that diazene binding occurs prior to H_2 elimination, and the negative entropy of activation and inverse kinetic isotope effect indicate that H−H bond formation is the rate-limiting step. Thus, substrate binding causes reductive elimination of H_2 that formally reduces the metals, and the metals use the additional two electrons to cleave the N−N multiple bond.

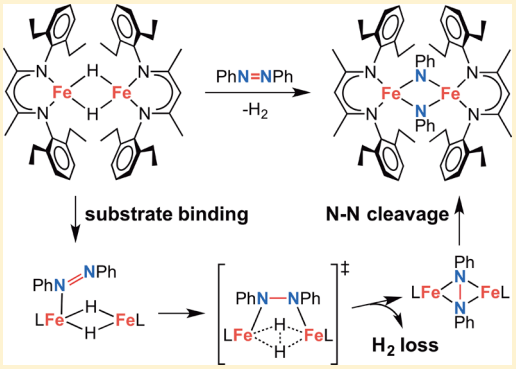

INTRODUCTION

Transition metals are responsible for some of the most impressive multielectron reducing reactions in chemistry, including large-scale reduction of triple bonds in N_2 (Haber−Bosch process and nitrogenase) and carbon monoxide (Fischer−Tropsch reaction). In each of these large-scale reductions, H_2 is intimately involved as a substrate or product of the reaction. Ongoing developments in research on nitrogenase suggest that it also uses H_2 strategically in its cleavage of strong bonds in substrates that include diazene, hydrazine, CO, CO_2, acetylene, and cyclopropenes.[1] According to recent papers, nitrogenase can store reducing electrons at the multimetallic active site as hydrides (note that a dihydride species has been detected in nitrogenase using ENDOR spectroscopy).[2−6] In this mechanism, dihydride reductively eliminates H_2 to generate a coordinatively unsaturated species in which the metals have been reduced by a total of two electrons, and the resulting reduced species can thus be generated without any strong reducing agents.[7] This strategy has also been used in other catalytic reactions, and has been reviewed recently by Fryzuk and by Quadrelli.[8]

In this paper, we focus on cleavage of the N−N double bond of azobenzene. There are a number of examples where transition metal and *f*-block metals cleave azobenzene,[9,10] but these reductions use metal complexes where the metal is in a low formal oxidation state.[11] Thus, the electrons come from the reduced metal. The product from reduction of RN═NR is typically an imido complex with a coordinated NR group. Metals with high oxidation states in the products (early transition metals) tend to form terminal imido products, while low oxidation state metals (late transition metals) tend to form bridging imido complexes when sterics allow.[12−14] Some synthetic 2Fe-2S clusters cleave azobenzene to form bridging imido groups in cubane-type products, showing that iron also prefers bridging.[15]

Herein, we use high-spin iron complexes supported by a bulky *β*-diketiminate ligand termed $L^{Me,Et}$ (Figure 1) that has not been used previously in iron chemistry. We show that iron(II)

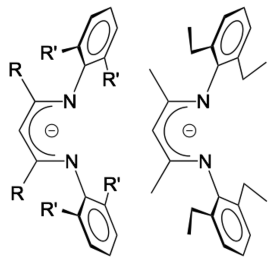

Figure 1. Left: General structure of *β*-diketiminate ligands, abbreviated $L^{R,R'}$ here. Right: the ligand $L^{Me,Et}$ used in this work.

Received: May 5, 2016
Published: September 6, 2016

ACS Publications © 2016 American Chemical Society

DOI: 10.1021/jacs.6b04654
J. Am. Chem. Soc. 2016, 138, 12112−12123

Scheme 1. Synthesis of Complexes 1−4

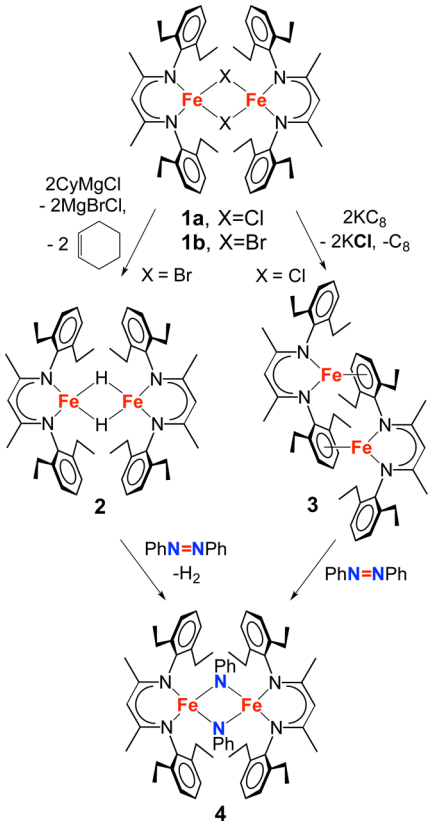

hydrides break the N−N double bond of azobenzene with elimination of H_2, and examine the reaction mechanism through kinetic studies. These studies are used to propose a mechanism in which substrate binding precedes (and enables) H_2 reductive elimination.

RESULTS

Synthesis and Characterization of Iron Complexes of $L^{Me,Et}$. In the literature, low-coordinate iron(I) and iron(II) halide complexes of other β-diketiminate ligands were produced by reduction of $[L^{R,R'}FeX]_2$ where $L^{R,R'}$ is illustrated in Figure 1 and X = Cl or Br.[16,17] In an analogous fashion, $[L^{Me,Et}FeCl]_2$ (**1a**) was synthesized by the deprotonation of $L^{Me,Et}H$ with benzylpotassium and addition of the resulting solution to $FeCl_2(THF)_{1.5}$ in THF. Heating in toluene at 90 °C for 18 h drives off THF, ultimately giving pure $[L^{Me,Et}FeCl]_2$ (**1a**) in 66% yield (**1a**, Scheme 1). A single crystal obtained from toluene was crystallographically characterized, and shows metrical parameters similar to other β-diketiminate complexes (Figure 2). The ^{1}H NMR spectrum of **1a** in C_6D_6 has seven paramagnetically shifted resonances as expected for D_{2h} symmetry. The Mössbauer parameters of solid **1a** at 80 K are δ = 0.91(2) mm/s and $|\Delta E_Q|$ = 2.54(2) mm/s, which are characteristic for high-spin iron(II) diketiminate centers with halide ligands.[17]

$[L^{Me,Et}FeBr]_2$ (**1b**) was synthesized similarly, though the process of heating in toluene had to be repeated multiple times to complete the precipitation of an off-white solid (presumably KBr) and the disappearance of a ^{1}H NMR resonance at δ −60.9 ppm. After this treatment, it was possible to isolate $[L^{Me,Et}FeBr]_2$ **1b** in 80% yield. The ^{1}H NMR spectrum of **1b** has resonances within 2 ppm of the resonances of **1a**. The Mössbauer parameters of solid **1b** at 80 K are δ = 0.88(2) mm/s and

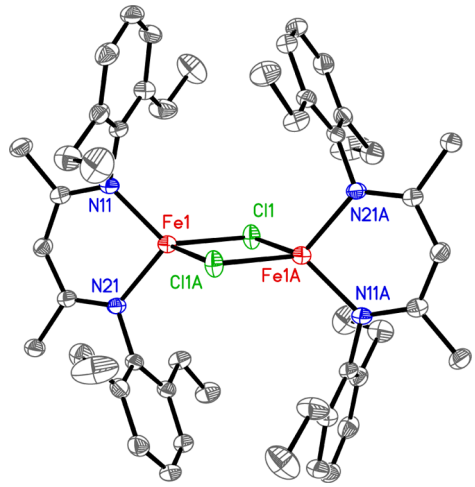

Figure 2. Molecular structure of **1a** with 50% thermal ellipsoids. Hydrogen atoms omitted for clarity. Selected bond distances (Å) and angles (deg): Fe(1)−N(11), 1.9811(13); Fe(1)−N(21), 1.9860(13); Fe(1)−Cl(1), 2.3402(5); Fe(1)−Cl(1A), 2.3418(5); N(11)−Fe(1)−N(21), 93.57(5); N(11)−Fe(1)−Cl(1), 120.65(4); N(21)−Fe(1)−Cl(1), 118.40(4). An alternative crystallization from THF/pentane gave the tetrahedral THF adduct $L^{Me,Et}Fe(Cl)(THF)$, for which the crystal structure is presented in the Supporting Information.

$|\Delta E_Q|$ = 2.55(2) mm/s. Though it has not been crystallographically characterized, we presume that **1b** is a dimer because its ^{1}H NMR and Mössbauer spectra are similar to those of **1a**.

Synthesis and Characterization of an Iron(II) Hydride Complex. Some β-diketiminate iron(II) hydride complexes have been synthesized by adding 2 equiv of (cyclohexyl)MgX (X = Cl or Br) to $[L^{R,R'}FeX]_2$ to form a transient Fe^{II}-cyclohexyl complex that undergoes β-hydride elimination to release cyclohexene.[22] $[L^{Me,Et}FeH]_2$ (**2**) was synthesized from **1b** by this method, and **2** crystallized from pentane in 74% yield. The X-ray crystal structure of **2** (Figure 3) shows a hydride-bridged dimer lying on a crystallographic inversion center. The unique hydride position was located in the difference Fourier map and its position was refined to give Fe−H bond lengths of 1.79(2) and 1.81(2) Å, which are within the known range for M−H

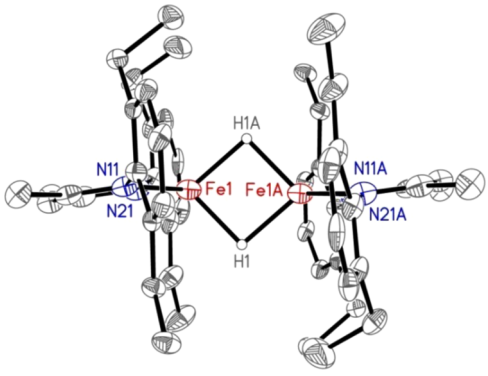

Figure 3. Molecular structure of **2** with 50% thermal ellipsoids. Hydrogen atoms on supporting ligand omitted for clarity. The crystallographically equivalent bridging hydride ligands were found in the difference Fourier map, and the position was refined. Selected bond distances (Å) and angles (deg): Fe(1)−N(11), 1.9908(12); Fe(1)−N(21), 1.9927(13); Fe(1)−H(1), 1.79(2); Fe(1)−Fe(1A), 2.6206(5); N(11)−Fe(1)−N(21), 94.38(5); N(11)−Fe(1)−H(1), 117.1(7); N(21)−Fe(1)−H(1), 121.5(7).

DOI: 10.1021/jacs.6b04654
J. Am. Chem. Soc. 2016, 138, 12112−12123

bonds but longer than previous (β-diketiminate)iron(II) hydride complexes (1.5−1.6 Å).[18] One possible explanation is that minor disorder between multiple positions in the 2Fe-2H core is masked by the inversion center.

The ^{1}H NMR spectrum of **2** in C_6D_6 exhibits seven sharp paramagnetic peaks between δ 10.5 ppm and −10.8 ppm, and their integrations are consistent with one symmetric ligand environment. Resonances for the hydrides are not seen in the ^{1}H NMR spectrum, which is expected due to their proximity to the paramagnetic iron centers. The two hydrogen atoms on each methylene carbon have different resonances because they are chemically inequivalent (see Supporting Information for an illustration). This phenomenon is also seen in complexes with $L^{Me,iPr}$ where the two methyls on the isopropyl groups are chemically inequivalent.[19] The solution magnetic moment is 5.2(2) BM per dimer, which is lower than the spin-only value expected for two uncoupled high-spin iron(II) ions ($\sqrt{2} \times 4.9 = 6.9\ \mu_B$). This is tentatively attributed to antiferromagnetic coupling between the two nearby (2.62 Å) iron atoms, which also explains the narrow chemical shift range of paramagnetic peaks in the ^{1}H NMR spectrum. The ^{1}H NMR spectrum was similar between C_6D_6 and THF-d_8 solutions (see Supporting Information), suggesting that THF does not coordinate and break up the dimeric structure.

Preparation and Characterization of a Dimeric Iron(I) Complex. Under an argon atmosphere, a THF solution of $[L^{Me,Et}FeCl]_2$ (**1a**) was treated with KC_8 to produce dark red crystals in 40% yield. X-ray crystallography revealed an iron(I) dimer (**3**) where a phenyl ring of each ligand is coordinated η^6 to the second iron. This geometry has been observed previously in β-diketiminate-supported Cu, Ni, and V dimers.[20−22] The crude ^{1}H NMR spectrum in C_6D_6 (Figure 4) features resonances at δ

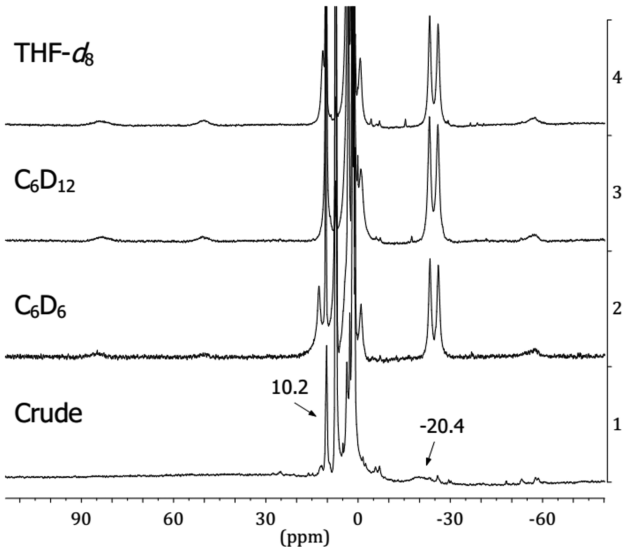

Figure 4. ^{1}H NMR spectra of **3** in C_6D_6, C_6D_{12}, and THF-d_8. The bottom spectrum is the crude reaction mixture formed from **1a** and KC_8 in C_6D_6.

10 ppm (sharp) and −20 ppm (very broad) that are reminiscent of the ^{1}H NMR chemical shifts of $L^{Me,iPr}Fe(C_6H_6)$ at δ 11 ppm (sharp) and −28 ppm (very broad),[23] suggesting that the kinetic product is a related monomeric arene complex of $L^{Me,Et}$Fe-(benzene), which then forms the thermodynamic product **3** during crystallization. The dimer **3** does not dissociate in solution, as shown by the similar ^{1}H NMR spectra in Figure 4,

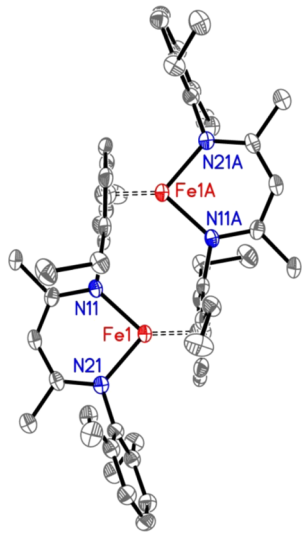

Figure 5. Molecular structure of **3**, showing 50% thermal ellipsoids. Hydrogen atoms omitted for clarity. Selected bond distances (Å) and angles (deg): Fe(1)−N(11), 1.953(3); Fe(1)−N(21), 1.974(2); Fe(1)−C(A), 2.114(3), 2.120(3), 2.122(3), 2.182(3), 2.193(3), 2.213(3); Fe(1)−Fe(1A), 4.1744(9); N(11)−Fe(1)−N(21), 92.00(10).

and reaction of **3** with 1 atm of H_2 at 60 °C for 8 h gives slow decomposition without any formation of **2**.

In the solid state, **3** has two independent dimers that each lie on crystallographic inversion centers (Figure 5); thus, one-half of each $[L^{Me,Et}Fe]_2$ dimer is crystallographically unique. The Fe-arene bond lengths indicate η^6-coordination, with Fe−C bond distances of 2.114(3) to 2.213(3) Å. The related Fe(I)-arene monomer, $L^{Me,iPr}Fe(C_6H_6)$, has similar η^6-coordination of the benzene ligand with bond lengths 2.139(2) to 2.157(2) Å.[25] The ^{1}H NMR spectra of **3** are nearly identical in C_6D_6, toluene-d_8, THF-d_8, and C_6D_{12} (Figure 4), suggesting that THF does not coordinate to the iron center in solution. The temperature dependence of the solid-state magnetic moment of solid **3** (Figure 6) indicates two low-spin iron(I) sites ($S_{Fe} = 1/2$) with a weak exchange coupling of $J \sim -1$ cm^{-1} that is consistent with the long Fe−Fe distance of 4.17 Å. Note that $L^{Me,iPr}Fe(C_6H_6)$

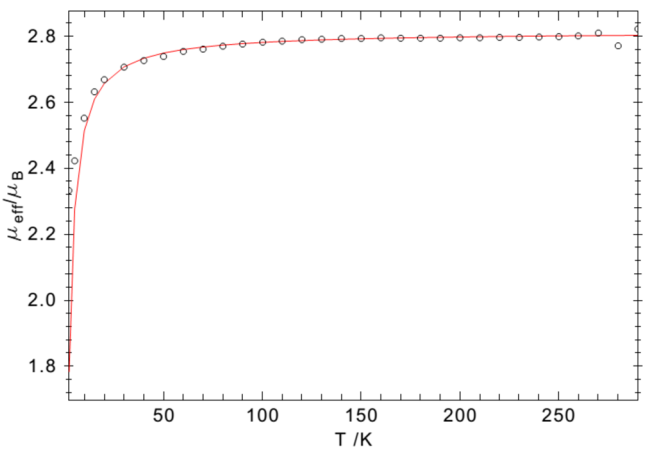

Figure 6. Variable temperature (2−300 K) solid-state magnetometry data of **3** with the fit (red line) for two $S = 1/2$ iron ions with $g_{average} = 2.28$, exchange coupling of $J = -1$ cm^{-1}, and a small intermolecular interaction parametrized with $\Theta_W = -1.6$ K.

DOI: 10.1021/jacs.6b04654
J. Am. Chem. Soc. 2016, 138, 12112−12123

also has a low-spin electronic configuration.[23] The magnetism $[L^{Me,Et}V]_2$ similarly indicated weak coupling ($J = -0.8$ cm^{-1}) of two $S = 1$ V(I) ions.[27]

Reactions with Azobenzene. Addition of one equivalent of azobenzene (PhN═NPh) to **2** or to **3** formed the same iron(III) imido dimer (**4**). The product mixtures were very clean as judged by ^{1}H NMR spectroscopy, and each product was isolated as crystals in 50−60% yield after crystallization. Crystals of **4** indicated the structure shown in Figure 7. The N−N

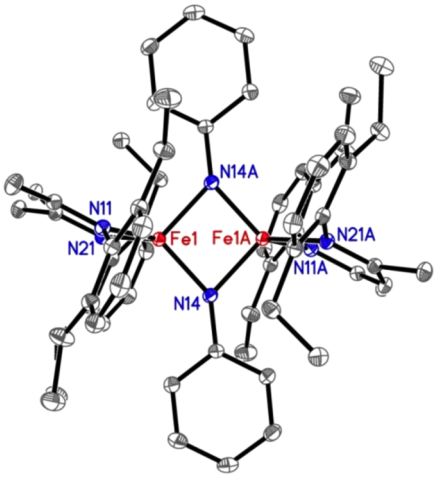

Figure 7. Molecular structure of **4**, showing 50% thermal ellipsoids. Hydrogen atoms omitted for clarity. Selected bond distances (Å) and angles (deg): Fe(1)−N(11), 2.019(1); Fe(1)−N(21), 2.034(1); Fe(1)−N(14), 1.878(1); Fe(1)−N(14A), 1.911(1); Fe(1)−Fe(1A), 2.5648(4); N(11)−Fe(1)−N(21), 92.00(4).

distance of 2.788(2) Å indicates the complete cleavage of the N−N double bond. The Fe−N(imido) bond lengths of 1.878(1) and 1.911(1) Å indicate Fe−N single bonds, as they are within the range of crystallographically characterized, low-coordinate Fe−N(amido) bond distances of 1.84(2) to 1.938(2) Å.[24]

The reaction of azobenzene with **2** produced H_2 in 100 ± 5% yield, as measured by gas chromatography. The production of H_2 has been observed in the reactions of the bulkier $[L^{Me,iPr}FeH]_2$ with other coordinating substrates (CO, isocyanide, and benzo[*c*]cinnoline), but no bond cleavage was observed in the iron(I) products.[25] On the other hand, the addition of azobenzene to monomeric $L^{tBu,iPr}$FeH results in the 1,2-insertion of azobenzene into the Fe−H bond to form a hydrazido complex.[26]

In order to experimentally gauge the ability to break up the dimers, we also performed the reaction of **2** with *m*-azotoluene (TolN═NTol), a close relative of azobenzene, which gave a product that is spectroscopically similar to **4**. When the reaction was repeated with a large excess of both PhN═NPh and TolN═NTol, the ^{1}H NMR spectrum of the product mixture contained only peaks previously observed in **4** and the *m*-azotoluene product. The lack of crossover suggests that the two halves of each azobenzene molecule end up in the same molecule of **4**.

The solution magnetic moment of **4** is 1.3(1) BM per dimer at room temperature, and the solid state magnetic response (Figure 8) fits to a model with two $S = 5/2$ iron ions having an antiferromagnetic exchange coupling of $J = -123$ cm^{-1}. The ^{1}H NMR spectrum of **4** in C_6D_6 consists of sharp resonances that

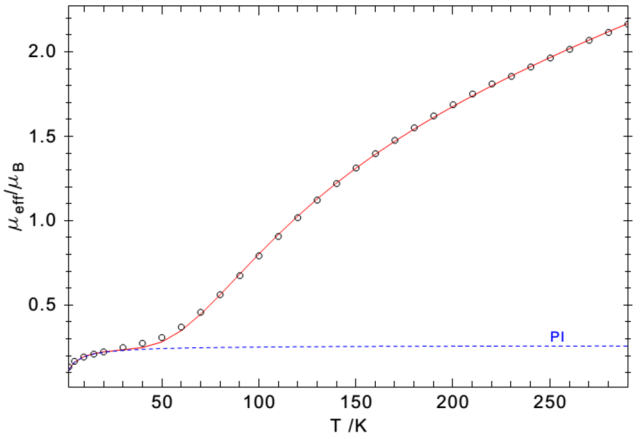

Figure 8. Variable temperature (2−300 K) solid-state magnetometry data of **4** with a fit (red line) for two $S = 5/2$ iron ions with exchange coupling of $J = -123$ cm^{-1}. The fit includes a contribution from a 0.2% paramagnetic impurity (PI) with spin $S_{PI} = 5/2$, indicated by the blue dashed line.

range from δ 19.5 to −14.3 ppm, consistent with paramagnetic excited states being populated at room temperature. The Mössbauer parameters of solid **4** at 80 K are $\delta = 0.38(2)$ mm/s and $|\Delta E_Q| = 1.10(2)$ mm/s, which are similar to other pseudotetrahedral β-diketiminate complexes having high-spin iron(III) centers.[22]

Benzo[*c*]cinnoline (BCC) has an N−N double bond that can only be *cis*. When 2 equiv of BCC was added to **2** or **3**, a BCC-bridged dimer (**5**) could be isolated as crystals in 86% isolated yield. The crystal structure of **5** (Figure 9) shows a dimer with each diazene ligand bound μ-κ^1:κ^1 and the N−N bond lengthened to 1.375(1) Å, which indicates a bond order between 1 and 2.[27] This is quite different from the product reported from reaction of BCC with $(L^{Me,iPr}Fe)N_2$; this reaction gave a monomer with the N−N double bond coordinated side-

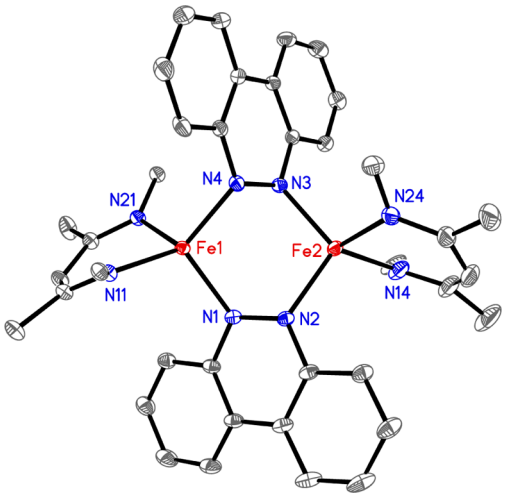

Figure 9. Molecular structure of **5**, showing 50% thermal ellipsoids. Hydrogen atoms and *N*-aryl groups omitted for clarity. Selected bond distances (Å) and angles (deg): Fe(1)−N(11), 2.022(1); Fe(1)−N(21), 2.032(1); Fe(1)−N(1), 2.043(1); Fe(1)−N(4), 1.999(1); Fe(2)−N(14), 2.034(1); Fe(2)−N(24), 2.022(1); Fe(2)−N(2), 2.042(1); Fe(2)−N(3), 2.100(1); Fe(1)−Fe(2), 3.5725(4); N(1)−N(2), 1.372(1); N(3)−N(4), 1.375(1); N(11)−Fe(1)−N(21), 92.24(4); N(14)−Fe(2)−N(24), 92.67(5).

DOI: 10.1021/jacs.6b04654
J. Am. Chem. Soc. 2016, 138, 12112−12123

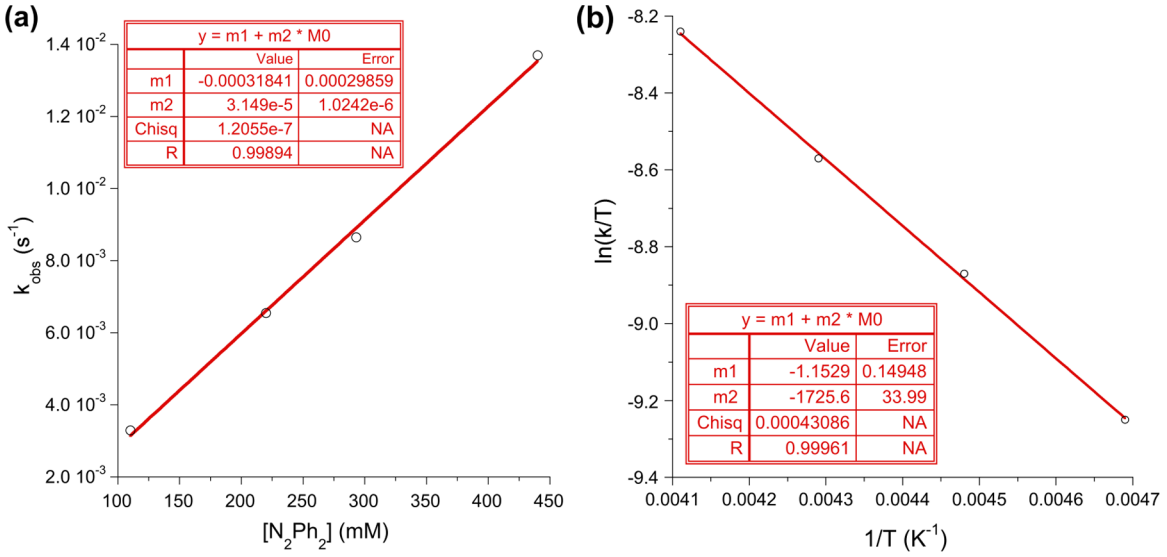

Figure 10. (a) The dependence of k_{obs} on $[N_2Ph_2]$ for the reaction between $[L^{Et}FeH]_2$ and excess azobenzene at −50 °C. (b) An Eyring plot for the same reaction at 440 mM azobenzene.

on (η^2) to a single iron (N═N, 1.385(2) Å).[30] Thus, the extent of N−N bond weakening is similar between the mononuclear and dinuclear species, despite the different binding modes. The observation of bridging coordination in the complex of $L^{Me,Et}$ may indicate a preference for end-on coordination of N═N ligands between two metals when sterics permit. In any case, no N═N cleaved products were observed from this reaction, indicating that the constrained geometry of BCC inhibits the N═N bond cleaving reaction.

Kinetic Studies. We were particularly intrigued by the reaction of the hydride complex **2** with azobenzene to form **4**, which releases H_2 and cleaves the N−N double bond. Mixtures of **2** and azobenzene (≥10 equiv) were monitored by UV−vis spectroscopy at various temperatures, and the observed rate constants were derived from the exponential fits of the absorbance at 750 nm over time. The growth of **4** and decay of **2** were also monitored using ^{1}H NMR spectroscopy, which showed no intermediates or byproducts. Varying the concentration of azobenzene revealed a linear dependence of the observed rate constant on $[N_2Ph_2]$ (Figure 10a). The combined data indicate the rate law in eq 1.

$$\text{Rate} = k[\mathbf{2}][N_2Ph_2] \quad (1)$$

Temperatures lower than −70 °C resulted in the precipitation of **4**, and temperatures higher than −30 °C were too fast to monitor accurately. Despite these limitations, the activation parameters determined from an Eyring analysis (Figure 10b) at temperatures −30 to −60 °C are $\Delta H^{\ddagger}$ = 3.43(6) kcal/mol and $\Delta S^{\ddagger}$ = −50(1) cal/mol·K, which yield $\Delta G^{\ddagger}_{298}$= 18.3(3) kcal/mol.

When flooding concentrations of N_2Ph_2 were added to the iron(I) dimer **3**, the ^{1}H NMR spectrum showed **4** and an additional product. Since the production of **4** from **3** could not be studied over a sufficiently wide range of conditions, kinetic studies of this alternative route to **4** were not pursued.

The deuteride analogue of **2**, $[L^{Me,Et}FeD]_2$ (**2-D**), was synthesized by treating **2** with D_2 gas, in a method that was previously established for closely related complexes.[28] Complete deuteration in **2-D** was clear by ^{1}H NMR spectroscopy, because the ligand resonances in **2-D** are shifted from those in **2** by the paramagnetic isotope effect on chemical shift (PIECS).[29] Four parallel kinetic experiments (side-by-side reactions of **2** and **2-D** deuterated from the same stock solution of **2**) were performed with N_2Ph_2 concentrations ranging from 50−440 mM. In each of the four independent iterations, the observed rate constant was greater for **2-D** than **2**, clearly indicating an *inverse* kinetic isotope effect with k_H/k_D = 0.86 ± 0.06 (standard deviation; see Supporting Information).

We also studied the kinetics of the reaction between **2** and benzo[*c*]cinnoline (BCC), to examine the effect of the constrained *cis* conformation of its N−N double bond. ^{1}H NMR spectroscopy shows that an excess of BCC reacts with **2** quickly to quantitatively form an intermediate which then converts to **5**. (No **3** was formed in this reaction.) We were unable to isolate the transient intermediate, but we performed kinetic studies on the slower step (see Supporting Information). These indicated the rate law shown in eq 2. The inverse dependence of the rate on [BCC] suggests that the intermediate could be a be a monometallic species, $L^{Me,Et}Fe(BCC)_2$, which reversibly dissociates one molecule of BCC and then forms **5** through a bimetallic rate-limiting step. Since this reaction did not give N−N double bond cleavage, details are relegated to the Supporting Information.

$$\text{Rate} = k[\text{Fe}]^2[\text{BCC}]^{-1} \quad (2)$$

Mechanistic Considerations. The rate law in eq 1 is an important constraint on the possible mechanisms for the N−N double bond cleavage of azobenzene by **2**. For example, rate-limiting initial dissociation or ring-opening of the hydride dimer **2** are inconsistent because they would give a rate with no dependence on the azobenzene concentration. Likewise, initial irreversible H_2 reductive elimination is inconsistent with the rate dependence on $[N_2Ph_2]$, with the stability of **2** in the absence of azobenzene, and with the lack of crossover of aryl groups in **4** described above. Each of the aforementioned mechanisms is also inconsistent with the large negative entropy of activation of −50 cal/mol·K.

Scheme 2 outlines two mechanisms that are consistent with the rate law and activation parameters. For azobenzene to be part of the rate-limiting step, it must first coordinate to **2**. This

DOI: 10.1021/jacs.6b04654
J. Am. Chem. Soc. 2016, 138, 12112−12123

Scheme 2. Possible Mechanisms for the Cleavage of N_2Ph_2 by 2[a]

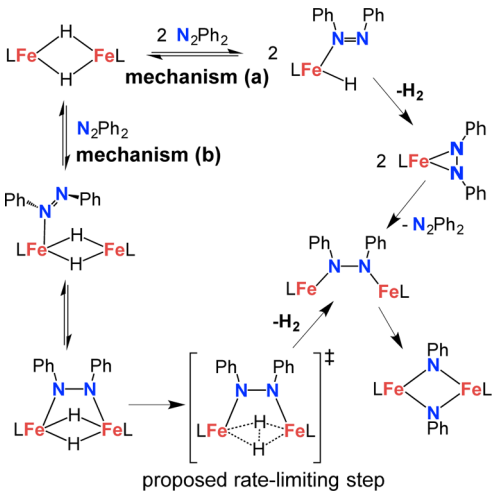

[a]Mechanism (b) is more consistent with the data, as described in the text. A proposed transition state for the rate-limiting step in mechanism (b) is drawn, but the bonding in this species is not clear from the kinetics studies (H_2 could be bound to only one Fe atom).

coordination could break the dimer of **2** to form LFe(H)-(N_2Ph_2) (mechanism *a*), or coordination could occur without dimer cleavage (mechanism *b*). One argument against mechanism *a* is that the intermediate $L^{Me,Et}Fe(H)(N_2Ph_2)$ would be expected to undergo rapid [1,2]-insertion, as observed in the addition of azobenzene to $[L^{tBu,iPr}FeH]_2$.[31,30] However, this hypothesis must still be considered because the steric differences of the supporting ligand could influence the reactivity. However, mechanism *a* predicts a normal kinetic isotope effect ($k_H/k_D > 1$) on the rate of dimer cleavage, in conflict with the data above.

Mechanism *b* predicts a primary KIE only if the elimination of H_2 is part of the rate-limiting step.[31] The reductive elimination of H_2 from dihydride complexes has been observed to give inverse kinetic isotope effects like those observed here.[32,33] The inverse kinetic isotope effect could correspond to a late transition state for H−H bond formation in which the high-frequency H−H bond is mostly formed, or could reflect an equilibrium with a transient H_2 complex.[34] The kinetics do not show whether the hydrides in the intermediate are connected to one or both iron atoms.

The fact that no intermediates are observed requires that the steps before this rate-limiting step (including the binding of azobenzene) are endoergic and reversible. We also note that azobenzene is predominantly *trans* at equilibrium, but presumably needs to isomerize to *cis* in order to bridge the metals. In an effort to test this idea, we photogenerated *cis*-azobenzene and observed that it is rapidly isomerized to *trans*-azobenzene under reaction conditions. However, the imido dimer product (**4**) also rapidly catalyzed the conversion of *cis*-azobenzene to *trans*-azobenzene, so we cannot rule out the possibility that the isomerization occurs after formation of product. Thus, we are unable to draw solid mechanistic conclusions regarding *cis*/*trans* isomerization during the pathway.

DFT Calculations of the Mechanism. The transformation of **2** to **4** was also evaluated by way of DFT calculations, to provide an additional gauge of the feasibility of the proposed mechanisms in Scheme 2. After testing several possible functionals (see Supporting Information), the B3LYP[35] functional was chosen for these studies, using the triple-ζ valence basis set def2-TZVP for the iron atoms and the atoms coordinated to them, and the double-ζ valence basis set def2-SVP on all other atoms. The mechanism was tested with a truncated β-diketiminate ligand $N_2C_3H_5$ and truncated *trans*-azobenzene (N_2H_2) because use of the full ligands was too computationally expensive. The unrealistic steric effects are of course expected to influence the energies of intermediates, but they are useful because they show a feasible pathway for N−N bond cleavage in this system.

The first step of mechanism *a* is the splitting of the hydride dimer with coordination of azobenzene to give $L^{trunc}Fe(H)$-(N_2H_2). This step was calculated to be endergonic by 16.6 kcal/mol, and would probably be even more unfavorable without truncation of the ligand.

A specific pathway for mechanism *b* is outlined in Figure 11, where the superscripts indicate the spin multiplicities. The first step of the mechanism is the coordination of *trans*-diazene to the hydride dimer to give an adduct **B**. The lowest-energy geometry and spin state (^{7}**B-*trans***) had η^1 coordination to a single iron. Binding of azobenzene was very weak (ΔG = −0.6 kcal/mol), consistent with this step being reversible.

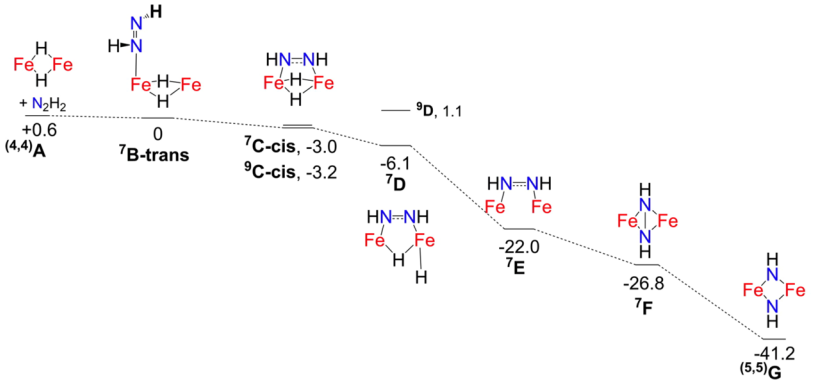

Figure 11. Calculated mechanism of N=N bond cleavage of diazene when added to **2** with a truncated supporting ligand. Superscripts indicate the multiplicities (2*S*+1), and broken-symmetry solutions are denoted (*x*,*x*) where *x* is the number of unpaired electrons on each half of the magnetically coupled molecule. Energies are given as $\Delta G°$ in kcal/mol. Ground state energies are relative to ^{7}**B-*trans***. Free H_2 is omitted from the diagram after reductive elimination but its energy was included in the thermodynamics.

DOI: 10.1021/jacs.6b04654
J. Am. Chem. Soc. 2016, 138, 12112−12123

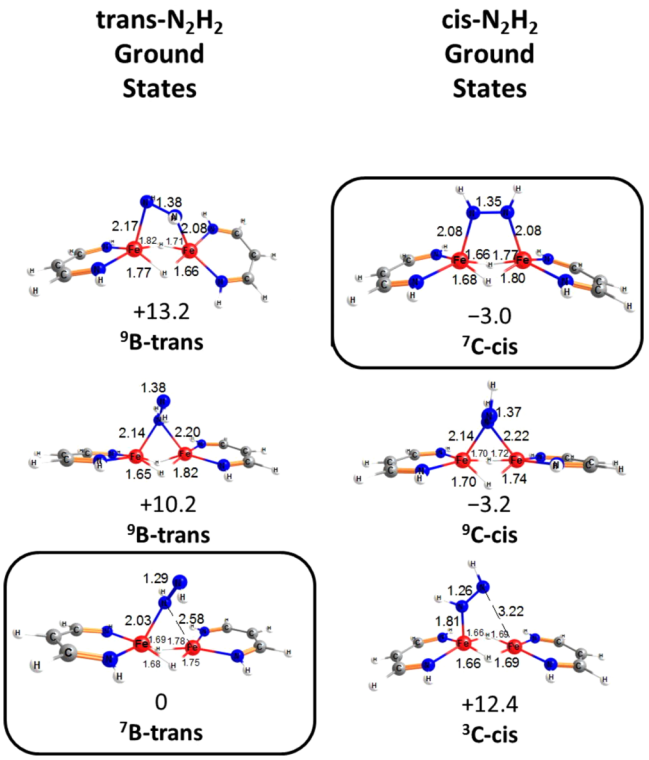

Figure 12. Lowest energy ground states for N_2H_2 adducts of **2**. Superscripts indicate the multiplicities (2*S*+1). The left column consists of the *trans*-diazene ground states, and the right column has the *cis*-diazene ground states. Energies are given as ΔG° in kcal/mol relative to ^{7}**B-*trans***.

Figure 12 shows the lowest energy geometries for *trans*-diazene and *cis*-diazene complexes in these truncated models. The isomerization of *trans* to *cis* was slightly favorable: ^{7}**C-*cis*** is calculated to be 3.0 kcal/mol lower in energy than ^{7}**B-*trans***. The *cis*-diazene optimized to a μ−η^1:η^1 binding mode with an NN bond distance of 1.34 Å and an NN stretching frequency of 1205 cm^{-1}. ^{9}**C-*cis*** is isoenergetic to ^{7}**C-*cis***, but we favor the septet because no spin state change is required.

The next calculated intermediate is ^{7}**D**, which possesses one terminal and one bridging hydride; this complex is 3.1 kcal/mol lower in free energy than ^{7}**C-*cis***. One of the hydride ligands moves to one iron to become a terminal hydride while the other hydride remains bridging between to two iron metals. Next is ^{7}**E**, which also has a partially activated N−N bond with an N═N bond length of 1.34 Å (1257 cm^{-1}). The overall loss of H_2 through this mechanism is very thermodynamically favorable, with ^{7}**E** lower in free energy than ^{7}**C-*cis*** by 19.0 kcal/mol. The lengthened N−N bonds in ^{7}**C-*cis*** and ^{7}**E** are reminiscent of those in the isolated complex **5** (which has a similar μ−η^1:η^1 bridging mode, Figure 9) where the N═N bond of BCC is lengthened to 1.37 Å.

Without hydride ligands, the diazene bridge can rotate from μ−η^1:η^1 to μ−η^2:η^2 in intermediate **F**. The ground state is ^{7}**F**, which is −4.8 kcal/mol lower in energy than ^{7}**E**. Its N−N bond length is 1.45 Å (937 cm^{-1}) indicating reduction of the NN bond further to a single bond. This bridging coordination of N═N/N—N ligands is known in iron complexes[16a,16c,36] and nickel complexes.[37] Saouma et al. have characterized diiron complexes with bridging N≡N, HN═NH, and H_2N—NH_2 ligands, using tripodal phosphine supporting ligands.[38] The N−N bond is then completely cleaved to give the bis-imido complex $^{(5,5)}$**G** where the NN distance is 2.55 Å, in agreement with the NN distance of 2.56 Å in **4**. Broken-symmetry methods indicated that the two iron(III) ions have strong antiferromagnetic coupling, in agreement with experiment. Details on the metal−metal interaction are given in the Supporting Information.

Thus, DFT calculations outline a reasonable pathway for mechanism *b* to cleave the N−N bond, which is consistent with all of the experimental data. Because of the use of truncated ligands, the energetic details of this mechanism are not likely to be accurate; however, the ability to identify a pathway without high-energy intermediates helps to elucidate the best geometries for H_2 elimination and N−N double bond cleavage in this diiron system.

Comparison to Literature. The ability of the diiron(I) complex **3** to perform the net four-electron reduction of a diazene to two imido groups in **4** has precedents in the chemistry of other monovalent β-diketiminate complexes.[39] In particular, Theopold and Tsai have reported analogous azobenzene cleavage reactions starting from vanadium(I) and chromium(I) precursors.[40] Warren has reported the formation of a diketiminate-supported bis-imidodicobalt(III) complex $[L^{Me,Me}Co(\mu\text{-Nxyl})]_2$ (xyl =2,6,-dimethylphenyl) from a cobalt(I) precursor, which was generated from an organic azide rather than from diazene N−N cleavage.[41] They also reported double bond cleavage of an N−O bond in a nitrosoarene to give a (μ-oxo)(μ-imido)dicobalt(III) complex, a more closely analogous reaction to the one described here.

The main relevance of the current work is the ability of the hydride complex **2** to release H_2 with diazene binding. Ligand-induced H_2 reductive elimination is well-known in organometallic systems.[8,26] Here, reductive elimination of H_2 formally leaves two electrons on the metal centers, and these electrons are used for diazene reduction. In a related reaction, Ohki and co-workers reported treating Cp*Fe{N($SiMe_3$)$_2$} and PhN═NPh with pinacolborane (HBpin) to give the N−N cleaved product $[Cp^*Fe(\mu\text{-NPh})]_2$.[42] They speculated that HBpin first reacted with the amido complex to give a transient unobserved iron(II) hydride complex Cp*FeH that could reductively eliminate H_2 cleave the N−N double bond to give the bis(imido) product. The mechanistic studies reported here show that this mechanism is reasonable.

Other notable work in the area comes from Qu and co-workers, who have described $[Cp^*Fe(\mu\text{-SR})]_2$ dimers that catalytically cleave the N−N bonds of hydrazines to give amines or ammonia.[43] In several cases, bridging *cis*-diazene ligands were observed, which can be protonated to give hydrazido complexes with formal oxidation of the metal center. Crystallography and DFT calculations showed a μ−η^1:η^2-N_2H_2R intermediate in the N−N cleaving process.[43c] Since the system described here has a low coordination number, our calculations indicate that it accesses a μ−η^2:η^2-N_2R_2 intermediate instead. From here, cleavage is akin to interconversions between μ−η^2:η^2-peroxo and bis(μ-oxo)dimetal systems, which are well-understood in the literature.[44]

We previously reported cleavage of the N−N double bond of N_2Ph_2 with $[L^{tBu,iPr}Fe(\mu\text{-H})]_2$, but in that case the product was $L^{tBu,iPr}$FeNHPh, in which the H atoms of the hydride were incorporated into the product.[45] In that reaction, rapid cleavage of the $Fe_2(\mu\text{-H})_2$ core gave monomeric iron(II) hydride intermediates that added across the N−N double bond to give the hydrazido complex $L^{tBu,iPr}$FeNPhNHPh as an isolable intermediate. Kinetic and other mechanistic studies on the

DOI: 10.1021/jacs.6b04654
J. Am. Chem. Soc. 2016, 138, 12112−12123

subsequent N−N single bond cleavage implicated a radical chain mechanism. The reaction reported here gives quite different products, and the main difference is that the $Fe_2(\mu\text{-}H)_2$ core in $L^{Me,Et}$-supported complexes does not break up into monomers, as shown by the rate law described above.[46] Maintaining the two hydrides in close proximity enables them to form a new H−H bond, releasing two electrons for use in substrate reduction.

Implications. In this system, the reductive elimination of H_2 does not occur prior to substrate binding, as shown by the rate law and by the solution stability of **2** in the absence of azobenzene. It is crucial that reductive elimination of H_2 from **2** is *brought about* by substrate binding, as we previously observed during addition of CO, isocyanides, and other strong donors to a related iron(II) hydride complex.[26] It is interesting to compare this to nitrogenase, where obligate H_2 production from hydrides is coupled to substrate reduction.[7,12] The structure of **2** has two bridging hydrides, similar to the E_4 (N_2-binding) state of the FeMoco.[47] Because of its ability to cleave an N−N multiple bond, **2** can be considered a functional model of a key step in nitrogenase even though its supporting ligands and geometry are different. Note that nitrogenase cleaves N_2H_2 as a substrate, though the mechanism is not established.[48] Importantly, the reaction described here mimics the hypothesized function of the reductive elimination in the enzyme: to provide two electrons and an open site for cleavage of a strong N−N bond.[4] This strategy has broader applicability, as emphasized in some recent reviews.[8]

Seefeldt and Hoffman have reported that loss of H_2 from the E_4 intermediate of nitrogenase has a normal kinetic isotope effect of 3−4,[2b] which differs from the inverse kinetic isotope effect of 0.9 observed in our synthetic system. In the literature, KIE values for reductive eliminations of H_2 vary,[32,33] and the variation from normal to inverse is described either by the difference between early and late transition states, or as an increasing contribution from the equilibrium isotope effect in a rapid pre-equilibrium with an unobserved H_2 complex.[34] These possibilities should be considered in the enzyme, as well as the idea that the rate-limiting step in the enzymatic release of H_2 by E_4 may be the migration of a hydride that would be more likely to give a normal kinetic isotope effect.

CONCLUSIONS

The β-diketiminate ligand $L^{Me,Et}$ supports novel iron complexes, including a high-spin iron(II) hydride dimer and a low-spin iron(I) dimer. Both of these complexes react with azobenzene to give a diiron(III) complex with two bridging imido ligands, which results from complete N−N double bond cleavage. The reaction from the hydride has been examined with kinetic studies and computations, which point toward a mechanism in which diazene binding precedes rate-limiting H_2 elimination. Thus, binding of the substrate brings about H_2 reductive elimination, which in turn gives additional electrons to use for cleavage of the substrate. This paradigm may be useful for understanding the role of hydrides in nitrogenase, and may contribute to strategies for other small-molecule activation reactions as well. In addition, the computational suggestion of intermediate structures, and the inverse kinetic isotope effect, may assist in design and testing of further systems for bond cleavage by hydride complexes.

EXPERIMENTAL SECTION

General Considerations. Unless otherwise specified, all manipulations were performed under an inert atmosphere using standard Schlenk techniques or in an M. Braun Unilab N_2-filled glovebox maintained at or below 1 ppm of O_2 and H_2O. Glassware was dried at 150 °C overnight. Toluene and pentane was purified by passage through activated alumina and Q5 columns from Glass Contour Co. (Laguna Beach, CA). THF was dried by distilling from Na/benzophenone. THF-d_8, toluene-d_8, C_6D_6, and 1,4-dioxane were dried over CaH_2 and then over Na/benzophenone and vacuum transferred and stored over 3 Å molecular sieves.

Azobenzene was purchased from Sigma-Aldrich and purified under inert atmosphere by filtering a hexane solution through activated alumina. Benzo(c)cinnoline (BCC) was purchased from Acros Organics. D_2 (99.8%) was purchased from Cambridge Isotope Laboratories. Cyclohexylmagnesium chloride (2.0 M in diethyl ether) was purchased from Sigma-Aldrich and titrated to determine the concentration.[49] $L^{Me,Et}H$,[50] benzylpotassium,[51] and $FeCl_2(THF)_{1.5}$[52] were synthesized by literature procedures. Anhydrous $FeBr_2$ was prepared from Fe and concentrated HBr in MeOH, and dried at about 200 °C under vacuum for 12 h prior to use.[49] Celite was dried at 250 °C under vacuum overnight. KC_8 was prepared by heating potassium and graphite at 150 °C under an argon atmosphere.

^1H NMR and ^{13}C NMR spectra were recorded on a Bruker Avance 500 MHz spectrometer or a Bruker Avance 400 spectrometer (400 MHz) at room temperature. Shifts (δ) are reported in ppm, relative to residual protiated solvent in C_6D_6 (δ 7.15 ppm), toluene-d_8 (δ 2.09 ppm), or THF-d_8 (δ 1.73, 3.58 ppm). Peaks were singlets unless otherwise noted. Solution magnetic susceptibilities were determined by Evans' method.[53] Infrared data were obtained on a Shimadzu FT-IR Prestige-21 spectrometer using KBr pellets. Electronic spectra were recorded between 400 and 1000 nm on a Cary 50 UV−visible spectrophotometer, using Teflon-sealed air-free cuvettes of 0.1 cm optical path length. The spectrometer was fitted with a Unisoku Scientific Instruments CoolSpek variable temperature system to maintain a constant temperature for kinetics experiments. Elemental analyses were performed by the CENTC Elemental Analysis Facility at the University of Rochester.

Headspace gas analyses were performed using a Thermo Scientific Trace 1300 gas chromatograph. Reactions were stirred under an N_2 atmosphere in 5 mL toluene in a 25 mL round-bottom flask sealed with a 180° vacuum adaptor capped with a rubber septum. At the beginning of the reaction, 400 μL of methane was injected into the headspace. After 30 min, a 250 μL gastight Hamilton syringe was used to draw 200 μL of headspace through the stopcock of the vacuum adaptor and injected into an SSL injection port. The samples ran through a 5 Å molecular sieve PLOT capillary GC column (30 m length, 0.53 mm inner diameter, 30 μm average thickness) at 0.95 mL/min flow of N_2 carrier gas and a constant oven temperature of 35 °C. Samples were detected using a TCD detector set to negative polarity, 1 mL/min reference gas flow, 100 °C, and 150 °C filament. Samples were quantified using a calibration curve created by identical methods, injecting H_2 in quantities of 20, 40, 60, and 80, into the headspace of the flask.

Computations. DFT calculations were performed with the ORCA program package, version 2.8.0.[54] Calculations reported here employed the B3LYP[36] functional. The Ahlrichs triple-ζ-quality basis set with one set of polarization functions, def2-TZVP, was used for the iron atom and atoms directly coordinated to it.[55] The smaller polarized Ahlrichs double-ζ-quality basis set, def2-SVP, was used on all other atoms. The auxiliary basis set def2-SVP/J was used to speed the calculations through the resolution of identity (RIJCOSx) approximation.[56] An empirical van der Waals correction was applied to the DFT energy (VDW10).[57] The SCF calculations were tightly converged (TightSCF) with unrestricted spin (UKS) and geometry optimizations converged normally (Opt). Numerical frequency (NumFreq) calculations were performed on each complex to obtain the Gibbs free energy (in kcal/mol). All energies are reported as free energies in kcal/mol. Ground states had no imaginary frequencies larger than $50i$ cm^{-1}. All reasonable spin states were optimized for each complex. Plots of the unrestricted corresponding orbitals (UCOs)[58] (iso-electron density surfaces = 80−90%) were generated with Gabedit, version 2.3.9.[59]

DOI: 10.1021/jacs.6b04654
J. Am. Chem. Soc. 2016, 138, 12112−12123

X-ray Crystallography. Single crystals were placed onto the tip of a 0.1 mm diameter glass capillary tube or fiber and mounted on a Bruker SMART APEX II CCD Platform diffractometer for a data collection at 100.0(1) K.[60] A preliminary set of cell constants and an orientation matrix were calculated from reflections harvested from three orthogonal wedges of reciprocal space. The full data collection was carried out using Mo Kα radiation (graphite monochromator) with appropriate frame times ranging from 45 to 90 s with a detector distance of 4.00 cm. The structure was solved using SIR97[61] and refined using SHELXL-97.[62] A direct-methods solution was calculated which provided most non-hydrogen atoms from the E-map. Full-matrix least-squares/difference Fourier cycles were performed which located the remaining non-hydrogen atoms. All non-hydrogen atoms were refined with anisotropic displacement parameters. All hydrogen atoms were placed in ideal positions and refined as riding atoms with relative isotropic displacement parameters. Tables with relevant parameters are in the Supporting Information.

Solid-State Magnetic Susceptibility. Powder magnetic susceptibility data were measured in the temperature range 2−300 K by using a SQUID susceptometer with a field of 1.0 T (MPMS-7, Quantum Design, calibrated with standard palladium reference sample). The experimental data were corrected for underlying diamagnetism by use of tabulated Pascal's constants, as well as for temperature-independent paramagnetism. The susceptibility and magnetization data were simulated with our own routine for exchange coupled systems (julX, available from E.B.). The simulations are based on the usual spin-Hamilton operator for dinuclear complexes. Intermolecular interactions were considered by using a Weiss temperature, θ_W, as perturbation of the temperature scale, $kT' = k(T - \theta_W)$ for the calculation.

Mössbauer Spectroscopy. Each Mössbauer sample was loaded into a Delrin Mössbauer sample cup and loaded into the spectrometer at 77 K. Low temperature ^{57}Fe Mössbauer measurements were performed using a SEE Co. MS4Mössbauer spectrometer integrated with a Janis SVT-400T He/N_2 cryostat for measurements at 80 K with a 0.07 T applied magnetic field. Isomer shifts were determined relative to α-Fe at 298 K. All Mössbauer spectra were fit using the program WMoss (SEE Co.).

Kinetic Studies. A solution of **2** in toluene (0.20 mL, 10 mM, 2.0 μmol) was added to a 1 mm quartz cuvette. The cuvette was cooled to −78 °C in a cold well cooled with a dry ice/acetone bath. A solution of azobenzene in toluene (0.20 mL, 880 mM, 0.18 mmol) was added to the cooled cuvette. The cuvette was shaken and quickly inserted into a Unisoku UV−vis cryostat cooled to −50 °C. The reaction was scanned at 750 nm every 5 s for 500−2000 s. The procedure was repeated using 110, 220, and 300 mM final concentrations of azobenzene. The procedure was repeated using −30, −40, and −60 °C temperature settings. Plots were generated and analyzed with Kaleidagraph v4.1.1.[63] The data were fit to the general first-order integrated kinetic equation $[\mathbf{4}] = a + [b \exp(-k_{obs}\cdot t)]$, where a and b are constants and k_{obs} is the pseudo-first-order rate constant.

*[$L^{Me,Et}$FeCl]$_2$ (**1a**).* A solution of benzylpotassium (0.367 g, 2.82 mmol) in THF (20 mL) was added slowly (1−2 drops/s) to a solution of $L^{Me,Et}H$ (1.02 g, 2.82 mmol) in THF (30 mL). After stirring for 4 h, the resulting solution was added to $FeBr_2(THF)_{1.5}$ (0.800 g, 3.50 mmol) in THF (30 mL) via a dropping funnel at a rate of 1 drop/s at room temperature, and then heated to 60 °C and stirred overnight. The yellow mixture was filtered through Celite and dried under vacuum. The yellow solid was dissolved in toluene (75 mL) and heated at 90 °C for 18 h. This mixture was filtered, dried, and washed twice with pentane (10 mL) to yield **1a** as an orange powder (844 mg, 66%). ^{1}H NMR (500 MHz, C_6D_6): 11.5/10.0 (14H, CH_2CH_3 and *m*-Ar), −9.5/−10.7 (36H, CH_2CH_3 and CH_2CH_3), −15.8 (2H, βCH), −35.8 (12H, αCCH_3), −45.2 (4H, *p*-Ar). μ_{eff} (C_6D_6, 25 °C) = 8.2(4) BM per dimer. IR (KBr): 3067 (w), 2963 (s), 2933 (m), 2875 (m), 1927 (w), 1859 (w), 1793 (w), 1623 (w), 1524 (s), 1444 (s), 1376 (s), 1327 (m), 1261 (m), 1180 (m), 1108 (w), 1019 (w), 937 (w), 857 (m), 803 (m), 759 (s), 645 (w) cm^{-1}. UV−vis (toluene, ε in mM^{-1}cm^{-1}): 325 (43), 395 (3), 505 (0.4) nm. Anal. Calcd for $C_{50}H_{66}Cl_2Fe_2N_4$: C, 66.31, H, 7.35, N, 6.19. Found: C, 66.39, H, 7.35, N, 5.92. Zero-field Mössbauer (solid, 80 K): δ = 0.91(2) mm/s, $|\Delta E_Q|$ = 2.54(2) mm/s.

*[$L^{Me,Et}$FeBr]$_2$ (**1b**).* A solution of benzylpotassium (247 mg, 1.90 mmol) in THF (10 mL) was added slowly (1−2 drops/s) to a solution of $L^{Me,Et}H$ (690 mg, 1.90 mmol) in THF (15 mL). After stirring for 4 h, the resulting solution was added to $FeBr_2$ (489 mg, 2.27 mmol) in THF (15 mL) via a dropping funnel at a rate of 1 drop/s at room temperature, and then heated to 60 °C and stirred overnight. The yellow mixture was filtered through Celite and dried under vacuum. The yellow solid was dissolved in toluene (50 mL) and heated at 90 °C for 2 d. The following process was performed twice: the orange mixture was filtered, solvent removed, and the solid was redissolved in 50 mL toluene and heated at 90 °C for 1 d. This process progressively reduced the amount of an impurity in the ^{1}H NMR spectrum with a characteristic peak at δ −60.9 ppm. The mixture was filtered and the orange filtrate was dried under vacuum to give **1b** as an orange solid (755 mg, 80%). ^{1}H NMR (500 MHz, C_6D_6): 12.0 (16H, CH_2CH_3 and *m*-Ar), −9.4 (24H, CH_2CH_3), −10.7 (8H, CH_2CH_3), −16.3 (2H, βCH), −33.7 (12H, αCCH_3), −45.2 (4H, *p*-Ar). μ_{eff} (C_6D_6, 25 °C) = 7.5 (5) BM per dimer. IR (KBr): 3001 (m), 2961 (s), 2931 (s), 2876 (s), 2846 (m), 1914 (w), 1849 (w), 1789 (w), 1622 (m), 1524 (s), 1511 (s), 1440 (s), 1433 (s), 1376 (s), 1364 (s), 1326(s), 1263 (s) 1179 (s), 1108 (m), 1061 (w), 1023 (m), 937 (w), 897 (w), 856 (w), 804 (s), 759 (s) cm^{-1}. UV−vis (toluene, ε in mM^{-1}cm^{-1}): 325 (32), 405 (4), 510 (0.5) nm. Anal. Calcd for $C_{50}H_{66}Br_2Fe_2N_4$: C, 60.38, H, 6.69, N, 5.63. Found: C, 60.11, H, 6.74, N, 5.82. Zero-field Mössbauer (solid, 80 K): δ = 0.88(2) mm/s, $|\Delta E_Q|$ = 2.55(2) mm/s.

*[$L^{Me,Et}$FeH]$_2$ (**2**).* Cyclohexylmagnesium chloride (115 μL, 0.264 mmol, 2.3 M in Et_2O) was added to **1a** (132 mg, 0.132 mmol) in toluene with an immediate color change from orange to brown-red. After stirring for 2 h, 2 drops of 1,4-dioxane were added while stirring and the mixture was filtered through Celite. Volatile materials were removed under vacuum to afford a brown solid. The solid was dissolved in pentane, filtered, and concentrated to produce brown crystals (81.0 mg, 74%). ^{1}H NMR (500 MHz, C_6D_6): δ 10.5 (2H, βCH), 10.2 (12H, αCCH_3), 6.0 (8H, *m*-Ar), −1.6 (8H, CH_2CH_3), −5.6 (2H, βCH), −6.7 (24H, CH_2CH_3), −9.1 (8H, CH_2CH_3), −10.8 (4H, *p*-Ar). μ_{eff} (C_6D_6, 25 °C) = 5.2(2) BM per dimer IR (KBr): 3065 (w), 3025 (w), 2960 (s), 2932 (m), 2873 (m), 1921(w), 1847 (w), 1793 (w), 1527 (s), 1508 (m), 1447 (s), 1426 (m), 1382 (s), 1329 (m), 1281 (w), 1264 (m), 1182 (m), 1106 (w), 1022 (w), 1014 (w), 935 (w), 855 (w), 802 (m), 762 (m) cm^{-1}. UV−vis (toluene, ε in mM^{-1}cm^{-1}): 320 (27) nm. Anal. Calcd for $C_{50}H_{68}Fe_2N_4$: C, 71.77, H, 8.19, N, 6.70. Found: C, 71.62, H, 8.18, N, 6.60. Zero-field Mössbauer (solid, 80 K): δ = 0.66(2) mm/s, $|\Delta E_Q|$ = 1.27(2) mm/s.

*Synthesis of [L^{Et}FeD]$_2$ (**2-D**).* **2** (2.8 mg, 0.0033 mmol) was dissolved in toluene-d_8 (0.6 mL) to give a brown solution. The solution was transferred to a resealable flask. On the Schlenk line, the headspace was evacuated and replaced with 1 atm of D_2 gas three times. The flask was shaken for 2 min each time. ^{1}H NMR (C_6D_6, 25 °C): δ 11.4 (14H), 6.3 (8H), −1.4 (8 H), −5.7 (2H), −7.2 (24H), −9.6 (8H), −13.1 (4H) ppm.

*[$L^{Me,Et}$Fe]$_2$ (**3**).* A sample of **1b** (724 mg, 0.800 mmol) was dissolved in 17 mL THF under an atmosphere of argon. KC_8 (250 mg, 1.82 mmol) was added as a solid and the dark red mixture stirred for 30 min. The mixture was filtered and solvent was removed under vacuum. The dark red residue was dissolved in toluene (15 mL), filtered, concentrated to 7 mL, and cooled to −45 °C for 1 week to afford dark brown crystals of **3** (268 mg, 40%). ^{1}H NMR (500 MHz, C_6D_6): δ 83.5, 50.1, 12.6, 10.4, 3.1, 0.9, −1.0, −23.4, −26.1, −56.7 ppm. All peaks were extremely broad, and could not be integrated accurately. μ_{eff} (tol-d_8, 25 °C) = 2.1(2) BM per dimer. IR (KBr): 3060 (w), 2963 (m), 2930 (m), 2874 (m), 1917 (w), 1855 (w), 1792 (w), 1536 (s), 1442 (m), 1391 (s), 1321 (w), 1259 (w), 1171 (m), 1107 (w), 1022 (w), 934 (w), 862 (w), 826 (w), 805 (w), 769 (w) cm^{-1}. Anal. Calcd for $C_{50}H_{66}Fe_2N_4$: C, 71.94, H, 7.97, N, 6.71. Found: C, 71.93, H, 8.08, N, 6.63. Zero-field Mössbauer (solid, 80 K): δ = 0.72(2) mm/s, $|\Delta E_Q|$ = 0.82(2) mm/s.

*[$L^{Me,Et}$FeNPh]$_2$ (**4**).* Method A: A solution of azobenzene (24.0 mg, 0.132 mmol) in toluene (2 mL) was added to a solution of **2** (110.6 mg, 0.132 mmol) in toluene (5 mL). The dark solution was stirred for 30 min and the solvent was removed under reduced pressure. The solid

DOI: 10.1021/jacs.6b04654
J. Am. Chem. Soc. 2016, 138, 12112−12123

was redissolved in toluene, filtered, and stored at −40 °C to form crystals of **4** for a total yield of 75.6 mg (62%). Method B: A solution of azobenzene (21 mg, 0.12 mmol) in toluene (2 mL) was added to a solution of **3** (98 mg, 0.12 mmol) in toluene (7 mL). The dark solution was stirred for 10 min and the solvent was removed under reduced pressure to form **4** of high purity based on ^{1}H NMR spectroscopy. The solid was redissolved in toluene, filtered, concentrated, and cooled to 40 °C with vapor diffusion of pentane, giving **4** in two crops for a total yield of 62 mg (52%). ^{1}H NMR (500 MHz, C_6D_6) δ 19.5 (4H, *p*-Ar), 8.7 (8H, CH_2CH_3), 8.0 (2H, *p*-Ph(N)), 4.9/4.17 (16H, *m*-Ar and CH_2CH_3), 1.2 (24H, CH_2CH_3), −2.3 (12H, αCCH_3), −13.6/−14.3 (8H, *o*- and *m*-Ph(N)). μ_{eff} (C_6D_6, 25 °C) = 1.3(1) per dimer. IR (KBr): 3061 (w), 3041 (w), 2964 (s), 2929 (m) 2873 (m) 2850 (w) 1936 (w) 1918 (w) 1853 (w) 1775 (w) 1574 (w) 1526 (s) 1465 (m) 1441 (s) 1382 (s) 1328 (m) 1262 (s) 1176 (m) 1108 (w) 1069 (w) 1022 (m) 993 (w) 932 (w) 883 (w) 852 (w) 806 (m) 758 (s) cm^{-1}. UV−vis (toluene, ε in mM^{-1}cm^{-1}): 315 (40), 435 (13) nm. Anal. Calcd for $C_{62}H_{76}Fe_2N_6$: C, 73.22, H, 7.53, N, 8.26. Found: C, 73.22, H, 7.51, N, 8.06. Zero-field Mössbauer (solid, 80 K): δ = 0.38(2) mm/s, $|\Delta E_Q|$ = 1.10(2) mm/s.

*$[L^{Me,Et}Fe(BCC)]_2$ (**5**).* Benzo[*c*]cinnoline (34 mg, 0.19 mmol) in pentane (10 mL) was added to **3** (77 mg, 0.093 mmol) in pentane (5 mL). The solution was stirred for 3 h and was concentrated under reduced pressure until a precipitate started to form. The mixture was filtered and placed in a−40 °C freezer to afford black crystals of **5** (95 mg, 86%). ^{1}H NMR (500 MHz, C_6D_6) δ 178 (2H), 58.8 (4H), 43.4 (4H), 25.4 (8H), 8.7/7.9 (not integrated), 4.8 (12H), −5.9 (12H), −29.5 (8H), −34.5 (2H), −37.3 (12H), −68.4 (2H), −107 (2H), −256 (2H), −308 (2H) ppm. μ_{eff} (C_6D_6, 25 °C) = 6.5(3) BM per dimer. IR (KBr): 3063 (w), 2963 (m), 2928 (m), 2874 (w), 1595 (w), 1510 (m), 1462 (w), 1439 (m), 1422 (w), 1383 (s), 1323 (w), 1261 (w), 1229 (w), 1175 (w), 1105 (w), 1018 (w), 932 (w), 862 (w), 833 (w), 804 (w), 752 (m) cm^{-1}. UV−vis (hexane, ε in mM^{-1}cm^{-1}): 250(67), 325(33), 395(22), 590(4) nm. Anal. Calcd for $C_{74}H_{82}Fe_2N_8$: C, 74.36, H, 6.92, N, 9.38. Anal. Calcd for $C_{79}H_{94}Fe_2N_8$ (with cocrystallized pentane): C, 74.87, H, 7.48, N, 8.84. Found: C, 75.16, H, 7.54, N, 8.84. Zero-field Mössbauer (solid, 80 K): δ = 0.82 mm/s, $|\Delta E_Q|$ = 2.66 mm/s.

Formation of BCC Intermediate. A solution of **2** in THF-d_8 (0.30 mL, 10 mM, 0.0030 mmol) was transferred to a J. Young tube using a 1.0 mL syringe. A solution of BCC in THF-d_8 (0.30 mL, 400 mM, 0.12 mmol) was added to the tube. A ^{1}H NMR spectrum was collected at 1 h, indicating the presence of a new species. (THF-d_8, 25 °C): δ 16.4 (6H), 2.6 (12 H), −19.2 (4H), −42.6 (1H), −52.7 (8H), −70.9 (2H) ppm. Over the course of 18 h at room temperature, the new species converted to $[L^{Et}Fe(BCC)]_2$.

■ ASSOCIATED CONTENT

Supporting Information

The Supporting Information is available free of charge on the ACS Publications website at DOI: 10.1021/jacs.6b04654.

Additional spectral, crystallographic, and computational information (PDF)

Crystal data (CIF)

■ AUTHOR INFORMATION

Corresponding Author

*patrick.holland@yale.edu

Present Address

⊥School of Basic Science, Department of Chemistry, Rani Channamma University, Vidyasangama, PBNH-4, Belagavi, India.

Notes

The authors declare no competing financial interest.

■ ACKNOWLEDGMENTS

This work was supported by the National Institutes of Health (GM065313). T.R.C. acknowledges support by the U.S. Department of Energy, Office of Basic Energy Sciences, grant DE-FG02-03ER15387. We thank Andreas Göbels for collecting SQUID data, and Reza Jafari for his assistance with azobenzene isomerization.

■ REFERENCES

(1) (a) Burgess, B. K.; Lowe, D. J. *Chem. Rev.* **1996**, *96*, 2983. (b) Holland, P. L. Nitrogen Fixation, In *Comprehensive Coordination Chemistry II*; McCleverty, J., Meyer, T. J., Eds.; Elsevier: Oxford, 2004; Vol. *8*, p 569. (c) Hoffman, B. M.; Lukoyanov, D.; Yang, Z.-Y.; Dean, D. R.; Seefeldt, L. C. *Chem. Rev.* **2014**, *114*, 4041.

(2) (a) Igarashi, R. Y.; Laryukhin, M.; Dos Santos, P. C.; Lee, H.-I.; Dean, D. R.; Seefeldt, L. C.; Hoffman, B. M. *J. Am. Chem. Soc.* **2005**, *127*, 6231. (b) Lukoyanov, D.; Barney, B. M.; Dean, D. R.; Seefeldt, L. C.; Hoffman, B. M. *Proc. Natl. Acad. Sci. U. S. A.* **2007**, *104*, 1451. (c) Doan, P. E.; Telser, J.; Barney, B. M.; Igarashi, R. Y.; Dean, D. R.; Seefeldt, L. C.; Hoffman, B. M. *J. Am. Chem. Soc.* **2011**, *133*, 17329. (d) Lukoyanov, D.; Yang, Z.-Y.; Duval, S.; Danyal, K.; Dean, D. R.; Seefeldt, L. C.; Hoffman, B. M. *Inorg. Chem.* **2014**, *53*, 3688.

(3) Guth, J. H.; Burris, R. H. *Biochemistry* **1983**, *22*, 5111.

(4) Hoffman, B. M.; Lukoyanov, D.; Yang, Z.-Y.; Dean, D. R.; Seefeldt, L. C. *Chem. Rev.* **2014**, *114*, 4041.

(5) Yang, Z.-Y.; Khadka, N.; Lukoyanov, D.; Hoffman, B. M.; Dean, D. R.; Seefeldt, L. C. *Proc. Natl. Acad. Sci. U. S. A.* **2013**, *110*, 16327.

(6) Lukoyanov, D.; Yang, Z.-Y.; Khadka, N.; Dean, D. R.; Seefeldt, L. C.; Hoffman, B. M. *J. Am. Chem. Soc.* **2015**, *137*, 3610.

(7) (a) Thorneley, R. N. F.; Eady, R. R.; Lowe, D. J. *Nature* **1978**, *272*, 557. (b) Crabtree, R. H. *Inorg. Chim. Acta* **1986**, *125*, L7. (c) Leigh, G. J.; McMahon, C. N. *J. Organomet. Chem.* **1995**, *500*, 219. (d) Henderson, R. A. In *Recent Advances in Hydride Chemistry*; Peruzzini, M., Poli, R., Eds.; Elsevier: New York, 2001; pp 463−505. (e) Dance, I. *Biochemistry* **2006**, *45*, 6328.

(8) (a) Ballman, J.; Munhá, R. F.; Fryzuk, M. D. *Chem. Commun.* **2010**, *46*, 1013. (b) Jia, H.-P.; Quadrelli, E. A. *Chem. Soc. Rev.* **2014**, *43*, 547.

(9) (a) Tsai, Y.-C.; Wang, P.-Y.; Lin, K.-M.; Chen, S.-A.; Chen, J.-M. *Chem. Commun.* **2008**, 205. (b) Kilgore, U. J.; Yang, X.; Tomaszewski, J.; Huffman, J. C.; Mindiola, D. J. *Inorg. Chem.* **2006**, *45*, 10712. (c) Monillas, W. H.; Yap, G. P. A.; MacAdams, L. A.; Theopold, K. H. *J. Am. Chem. Soc.* **2007**, *129*, 8090. (d) Lockwood, M. A.; Fanwick, P. E.; Eisenstein, O.; Rothwell, I. P. *J. Am. Chem. Soc.* **1996**, *118*, 2762. (e) Tsai, Y.-C.; Wang, P.-Y.; Chen, S.-A.; Chen, J.-M. *J. Am. Chem. Soc.* **2007**, *129*, 8066. (f) Aubart, M. A.; Bergman, R. G. *Organometallics* **1999**, *18*, 811. (g) Kaleta, K.; Arndt, P.; Beweries, T.; Spannenberg, A.; Theilmann, O. *Organometallics* **2010**, *29*, 2604. (h) Milsmann, C.; Turner, Z. R.; Semproni, S. P.; Chirik, P. J. *Angew. Chem., Int. Ed.* **2012**, *51*, 5386.

(10) (a) Evans, W. J.; Kozimor, S. A.; Ziller, J. W. *Chem. Commun.* **2005**, 4681. (b) Diaconescu, P. L.; Arnold, P. L.; Baker, T. A.; Mindiola, D. J.; Cummins, C. C. *J. Am. Chem. Soc.* **2000**, *122*, 6108. (c) Peters, R. G.; Warner, B. P.; Burns, C. J. *J. Am. Chem. Soc.* **1999**, *121*, 5585. (d) Brady, E. D.; Clark, D. L.; Keogh, W.; Scott, B. L.; Watkin, J. G. *J. Am. Chem. Soc.* **2002**, *124*, 7007. (e) Warner, B. P.; Scott, B. L.; Burns, C. J. *Angew. Chem., Int. Ed.* **1998**, *37*, 959.

(11) (a) Wucherer, E. J.; Tasi, M.; Hansert, B.; Powell, A. K.; Garland, M.-T.; Halet, J.-F.; Saillard, J.-Y.; Vahrenkamp, H. *Inorg. Chem.* **1989**, *28*, 3564. (b) Bruce, M. I.; Humphrey, M. G.; Shawkataly, O. B.; Snow, M. R.; Tiekink, E. R. T. *J. Organomet. Chem.* **1986**, *315*, C51. (c) Bruce, M. I.; Humphrey, M. G.; Shawkataly, O. B.; Snow, M. R.; Tiekink, E. R. T. *J. Organomet. Chem.* **1987**, *336*, 199. (d) Tasi, M.; Powell, A. K.; Vahrenkamp, H. *Angew. Chem., Int. Ed. Engl.* **1989**, *28*, 318.

(12) Zarubin, D. N.; Ustynyuk, N. A. *Russ. Chem. Rev.* **2006**, *75*, 671.

(13) Sharp, P. R. *Dalton Trans.* **2000**, 2647.

(14) Eikey, R. A.; Abu-Omar, M. M. *Coord. Chem. Rev.* **2003**, *243*, 83.

DOI: 10.1021/jacs.6b04654
J. Am. Chem. Soc. 2016, 138, 12112−12123

(15) (a) Verma, A. K.; Lee, S. C. *J. Am. Chem. Soc.* **1999**, *121*, 10838. (b) Zdilla, M. J.; Verma, A. K.; Lee, S. C. *Inorg. Chem.* **2011**, *50*, 1551. (c) Duncan, J. S.; Zdilla, M. J.; Lee, S. C. *Inorg. Chem.* **2007**, *46*, 1071.
(16) (a) Stubbert, B. D.; Holland, P. L.; Adhikari, D.; Mindiola, D. J. *Inorg. Synth.* **2010**, *35*, 38. (b) Cowley, R. E.; Holland, P. L. *Inorg. Chem.* **2012**, *51*, 8352.
(17) Rodriguez, M. M.; Bill, E.; Brennessel, W. W.; Holland, P. L. *Science* **2011**, *334*, 780.
(18) Bau, R.; Teller, R. G.; Kirtley, S. W.; Koetzle, T. F. *Acc. Chem. Res.* **1979**, *12*, 176.
(19) Eckert, N. A.; Smith, J. M.; Lachicotte, R. J.; Holland, P. L. *Inorg. Chem.* **2004**, *43*, 3306.
(20) (a) Amisial, L. D.; Dai, X.; Kinney, R. A.; Krishnaswamy, A.; Warren, T. H. *Inorg. Chem.* **2004**, *43*, 6537. (b) York, J. T.; Young, V. G., Jr.; Tolman, W. B. *Inorg. Chem.* **2006**, *45*, 4191.
(21) Pfirrmann, S.; Yao, S.; Ziemer, B.; Stosser, R.; Driess, M.; Limberg, C. *Organometallics* **2009**, *28*, 6855.
(22) Chang, K.-C.; Lu, C.-F.; Wang, P.-Y.; Lu, D.-Y.; Chen, H.-Z.; Kuo, T.-S.; Tsai, Y.-C. *Dalton Trans.* **2010**, *40*, 2324.
(23) Smith, J. M.; Sadique, A. R.; Cundari, T. R.; Rodgers, K. R.; Lukat-Rodgers, G.; Lachicotte, R. J.; Flaschenriem, C. J.; Vela, J.; Holland, P. L. *J. Am. Chem. Soc.* **2006**, *128*, 756.
(24) (a) Chen, H.; Bartlett, R. A.; Rasika Dias, H. V.; Olmstead, M. M.; Power, P. P. *J. Am. Chem. Soc.* **1989**, *111*, 4338. (b) Chen, H.; Bartlett, R. A.; Olmstead, M. M.; Power, P. P.; Shoner, S. C. *J. Am. Chem. Soc.* **1990**, *112*, 1048. (c) Olmstead, M. M.; Power, P. P.; Shoner, S. C. *Inorg. Chem.* **1991**, *30*, 2547. (d) Panda, A.; Stender, M.; Wright, R. J.; Olmstead, M. M.; Klavins, P.; Power, P. P. *Inorg. Chem.* **2002**, *41*, 3909. (e) Andersen, R. A.; Faegri, K., Jr.; Green, J. C.; Haaland, A.; Lappert, M. F.; Leung, W.; Rypdal, K. *Inorg. Chem.* **1988**, *27*, 1782. (f) Stokes, S. L.; Davis, W. M.; Odom, A. L.; Cummins, C. C. *Organometallics* **1996**, *15*, 4521. (g) Siemeling, U.; Vorfeld, U.; Neumann, B.; Stammler, H. *Organometallics* **1998**, *17*, 483. (h) Siemeling, U.; Vorfeld, U.; Neumann, B.; Stammler, H.-G. *Inorg. Chem.* **2000**, *39*, 5159.
(25) Yu, Y.; Sadique, A. R.; Smith, J. M.; Dugan, T. R.; Cowley, R. E.; Brennessel, W. W.; Flaschenriem, C. J.; Bill, E.; Cundari, T. R.; Holland, P. L. *J. Am. Chem. Soc.* **2008**, *130*, 6624.
(26) Smith, J. M.; Lachicotte, R. J.; Holland, P. L. *J. Am. Chem. Soc.* **2003**, *125*, 15752.
(27) Holland, P. L. *Dalton Trans.* **2010**, *39*, 5415.
(28) Dugan, T. R.; Bill, E.; MacLeod, K. C.; Brennessel, W. W.; Holland, P. L. *Inorg. Chem.* **2014**, *53*, 2370.
(29) Heintz, R. A.; Neiss, T. G.; Theopold, K. H. *Angew. Chem.* **1994**, *106*, 2389.
(30) Bellows, S.; Cundari, T. R.; Holland, P. L. *Organometallics* **2013**, *32*, 4741−4751.
(31) There could in principle be a secondary KIE on the rate of azobenzene binding, but increases in the coordination number typically weaken and lengthen bonds to the metal, and so one would expect a normal kinetic isotope effect.
(32) Kinetic isotope effects as low as 0.5 have been seen: Packett, D. L.; Trogler, W. C. *Inorg. Chem.* **1988**, *27*, 1768.
(33) In some cases, H_2 reductive elimination gives normal kinetic isotope effects with the following values: (a) 2.9: Evans, J.; Norton, J. R. *J. Am. Chem. Soc.* **1974**, *96*, 7577. (b) 1.4: Bavaro, L. M.; Montangero, P.; Keister, J. B. *J. Am. Chem. Soc.* **1983**, *105*, 4977. (c) 1.4: Deutsch, P. P.; Eisenberg, R. *Organometallics* **1990**, *9*, 709. (d) 1.1: Wang, W.; Narducci, A. A.; House, P. G.; Weitz, E. *J. Am. Chem. Soc.* **1996**, *118*, 8654. (e) 2.0: Hascall, T.; Rabinovich, D.; Murphy, V. J.; Beachy, M. D.; Friesner, R. A.; Parkin, G. *J. Am. Chem. Soc.* **1999**, *121*, 11402.
(34) Parkin, G. *J. Labelled Compd. Radiopharm.* **2007**, *50*, 1088.
(35) (a) Becke, A. D. *J. Chem. Phys.* **1993**, *98*, 5648. (b) Lee, C. T.; Yang, W. T.; Parr, R. G. *Phys. Rev. B: Condens. Matter Mater. Phys.* **1988**, *37*, 785.
(36) (a) Little, R. G.; Doedens, R. J. *Inorg. Chem.* **1972**, *11*, 1392. (b) Doedens, R. J. *Inorg. Chem.* **1970**, *9*, 429. (c) Tasi, M.; Powell, A. K.; Vahrenkamp, H. *Angew. Chem., Int. Ed. Engl.* **1989**, *28*, 318. (d) Tasi, M.; Powell, A. K.; Vahrenkamp, H. *Chem. Ber.* **1991**, *124*, 1549. (e) Wucherer, E. J.; Tasi, M.; Hansert, B.; Powell, A. K.; Garland, M.-T.; Halet, J.-F.; Saillard, J.-Y.; Vahrenkamp, H. *Inorg. Chem.* **1989**, *28*, 3564. (f) Doedens, R. J.; Ibers, J. A. *Inorg. Chem.* **1969**, *8*, 2709. (g) Kuz'mina, L. G.; Bokii, N. G.; Struchkov, Y. T.; Arutyunyan, A. V.; Rybin, L. V.; Rybinskaya, M. I. *Zh. Strukt. Khim.* **1971**, *12*, 875. (h) Volkers, P. I.; Rauchfuss, T. B. *J. Inorg. Biochem.* **2007**, *101*, 1748. (i) Zimniak, A. *J. Organomet. Chem.* **2002**, *645*, 274. (j) Bahr, N.; Beckmann, E.; Mathaner, K.; Hunkler, D.; Keller, M.; Prinzbach, H.; Vahrenkamp, H. *Chem. Ber.* **1993**, *126*, 429. (k) Wu, C.-Y.; Chen, Y.; Jing, S.-Y.; Lee, C.-S.; Dinda, J.; Hwang, W.-S. *Polyhedron* **2006**, *25*, 3053.
(37) Köthe, C.; Metzinger, R.; Herwig, C.; Limberg, C. *Inorg. Chem.* **2012**, *51*, 9740.
(38) (a) Saouma, C. T.; Müller, P.; Peters, J. C. *J. Am. Chem. Soc.* **2009**, *131*, 10358. (b) Sokolov, A. Y.; Schaefer, H. F. *Organometallics* **2010**, *29*, 3271.
(39) Tsai, Y.-C. *Coord. Chem. Rev.* **2012**, *256*, 722.
(40) (a) Tsai, Y.-C.; Wang, P.-Y.; Chen, S.-A.; Chen, J.-M. *J. Am. Chem. Soc.* **2007**, *129*, 8066. (b) Monillas, W. H.; Yap, G. P. A.; MacAdams, L. A.; Theopold, K. H. *J. Am. Chem. Soc.* **2007**, *129*, 8090. (c) Tsai, Y.-C.; Wang, P.-Y.; Lin, K.-M.; Chen, S.-A.; Chen, J.-M. *Chem. Commun.* **2008**, 205.
(41) (d) Dai, X.; Kapoor, P.; Warren, T. H. *J. Am. Chem. Soc.* **2004**, *126*, 4798.
(42) Ohki, Y.; Takikawa, Y.; Hatanaka, T.; Tatsumi, K. *Organometallics* **2006**, *25*, 3111.
(43) (a) Li, Y.; Li, Y.; Wang, B.; Luo, Y.; Yang, D.; Tong, P.; Zhao, J.; Luo, L.; Zhou, Y.; Chen, S.; Cheng, F.; Qu, J. *Nat. Chem.* **2013**, *5*, 320. (b) Chen, Y.; Liu, L.; Peng, Y.; Chen, P.; Luo, Y.; Qu, J. *J. Am. Chem. Soc.* **2011**, *133*, 1147. (c) Chen, Y.; Zhou, Y.; Chen, P.; Tao, Y.; Li, Y.; Qu, J. *J. Am. Chem. Soc.* **2008**, *130*, 15250.
(44) Tolman, W. B. *Acc. Chem. Res.* **1997**, *30*, 227.
(45) Sadique, A. R.; Gregory, E. A.; Brennessel, W. W.; Holland, P. L. *J. Am. Chem. Soc.* **2007**, *129*, 8112.
(46) This is reasonable by analogy to the analogue $[L^{Me,iPr}FeH]_2$, for which detailed studies have shown that it does not access a monomer: (a) Yu, Y.; Brennessel, W. W.; Holland, P. L. *Organometallics* **2007**, *26*, 3217. (b) See also ref 45.
(47) Hoffman, B. M.; Lukoyanov, D.; Yang, Z.-Y.; Dean, D. R.; Seefeldt, L. C. *Chem. Rev.* **2014**, *114*, 4041.
(48) Barney, B. M.; McClead, J.; Lukoyanov, D.; Laryukhin, M.; Yang, T.-C.; Dean, D. R.; Hoffman, B. M.; Seefeldt, L. C. *Biochemistry* **2007**, *46*, 6784.
(49) Watson, S. C.; Eastham, J. F. *J. Organomet. Chem.* **1967**, *9*, 165.
(50) (a) Mindiola, D. J.; Holland, P. L.; Warren, T. H. *Inorg. Synth.* **2010**, *35*, 1−6. (b) Characterization of $L^{Me,Et}H$: Cheng, M.; Moore, D. R.; Reczek, J. J.; Chamberlain, B. M.; Lobkovsky, E. B.; Coates, G. W. *J. Am. Chem. Soc.* **2001**, *123*, 8738.
(51) (a) Schlosser, M.; Hartmann, J. *Angew. Chem., Int. Ed. Engl.* **1973**, *12*, 508. (b) Bailey, P. J.; Coxall, R. A.; Dick, C. M.; Fabre, S.; Henderson, L. C.; Herber, C.; Liddle, S. T.; Loroño-González, D.; Parkin, A.; Parsons, S. *Chem. - Eur. J.* **2003**, *9*, 4820.
(52) Kern, R. J. *J. Inorg. Nucl. Chem.* **1962**, *24*, 1105.
(53) Schubert, E. M. *J. Chem. Educ.* **1992**, *69*, 62.
(54) Neese, F. *ORCA*, version 2.8; Universität Bonn, Germany, 2011.
(55) Weigend, F.; Ahlrichs, R. *Phys. Chem. Chem. Phys.* **2005**, *7*, 3297.
(56) (a) Zein, S.; Kulik, L. V.; Yano, J.; Kern, J.; Zouni, A.; Yachandra, V. K.; Lubitz, W.; Neese, F.; Messinger, J. *Philos. Trans. R. Soc., B* **2008**, *363*, 1167. (b) Zein, S.; Duboc, C.; Lubitz, W.; Neese, F. *Inorg. Chem.* **2008**, *47*, 134. (c) Parker, D. J.; Hammond, D.; Davies, E. S.; Garner, C. D.; Benisvy, L.; McMaster, J.; Wilson, C.; Neese, F.; Bothe, E.; Bittl, R.; Teutloff, C. *J. Biol. Inorg. Chem.* **2007**, 101.
(57) (a) Grimme, S. *J. Comput. Chem.* **2004**, *25*, 1463. (b) Grimme, S. *J. Comput. Chem.* **2006**, *27*, 1787. (c) Grimme, S.; Antony, J.; Ehrlich, S.; Krieg, H. *J. Chem. Phys.* **2010**, *132*, 154104.
(58) Neese, F. *J. Am. Chem. Soc.* **2006**, *128*, 10213.
(59) Allouche, A.-R. *J. Comput. Chem.* **2011**, *32*, 174.
(60) *APEX2*, version 2012.4−3; Bruker AXS: Madison, WI, 2012.

DOI: 10.1021/jacs.6b04654
J. Am. Chem. Soc. 2016, 138, 12112−12123

(61) Altomare, A.; Burla, M. C.; Camalli, M.; Cascarano, G. L.; Giacovazzo, C.; Guagliardi, A.; Moliterni, A. G. G.; Polidori, G.; Spagna, R. *SIR97: A New Program for Solving and Refining Crystal Structures*; Istituto di Cristallografia, CNR: Bari, Italy, 1999.
(62) Sheldrick, G. M. *SHELXL-2012*; University of Göttingen: Göttingen, Germany, 2012.
(63) *Kaleidagraph*, 4.1; Synergy Software: Reading, PA, 2010.

DOI: 10.1021/jacs.6b04654
J. Am. Chem. Soc. 2016, 138, 12112−12123